

1 Potential underestimation of ambient brown carbon absorption
2 based on the methanol extraction method and its impacts on
3 source analysis

4
5 Zhenqi Xu^a, Wei Feng^a, Yicheng Wang^a, Haoran Ye^a, Yuhang Wang^b, Hong Liao^a,
6 Mingjie Xie^{a,*}

7
8 ^aCollaborative Innovation Center of Atmospheric Environment and Equipment
9 Technology, Jiangsu Key Laboratory of Atmospheric Environment Monitoring and
10 Pollution Control, School of Environmental Science and Engineering, Nanjing
11 University of Information Science & Technology, 219 Ningliu Road, Nanjing 210044,
12 China

13 ^bSchool of Earth and Atmospheric Sciences, Georgia Institute of Technology, Atlanta,
14 GA 30332, United States

15
16 *Corresponding to:

17 Mingjie Xie (mingjie.xie@nuist.edu.cn, mingjie.xie@colorado.edu);

18 Mailing address: 219 Ningliu Road, Nanjing, Jiangsu, 210044, China

28 **Abstract**

29 The methanol extraction method was widely applied to isolate organic carbon (OC)
30 from ambient aerosols, followed by measurements of brown carbon (BrC) absorption.
31 However, undissolved OC fractions will lead to underestimated BrC absorption. In this
32 work, water, methanol (MeOH), MeOH/dichloromethane (MeOH/DCM, 1:1, v/v),
33 MeOH/DCM (1:2, v/v), tetrahydrofuran (THF), and N,N-dimethylformamide (DMF)
34 were tested for extraction efficiencies of ambient OC, and the light absorption of
35 individual solvent extracts was determined. Among the five solvents and solvent
36 mixtures, DMF dissolved the highest fractions of ambient OC (up to ~95%), followed
37 by MeOH and MeOH/DCM mixtures (< 90%), and the DMF extracts had significant
38 ($p < 0.05$) higher light absorption than other solvent extracts. This is because the OC
39 fractions evaporating at higher temperatures ($> 280^{\circ}\text{C}$) are less soluble in MeOH (~80%)
40 than in DMF (~90%) and contain stronger light-absorbing chromophores. Moreover,
41 the light absorption of DMF and MeOH extracts of collocated aerosol samples in
42 Nanjing showed consistent temporal variations in winter when biomass burning
43 dominated BrC absorption. While the average light absorption of DMF extracts was
44 more than two times greater than the MeOH extracts in late spring and summer. The
45 average light absorption coefficient at 365 nm of DMF extracts was 30.7% higher ($p <$
46 0.01) than that of MeOH extracts. Source apportionment results indicated that the
47 MeOH solubility of BrC associated with biomass burning, lubricating oil combustion,
48 and coal combustion is similar to their DMF solubility. The BrC linked with unburned
49 fossil fuels and polymerization processes of aerosol organics was less soluble in MeOH
50 than in DMF, which was likely the main reason for the large difference in time series
51 between MeOH and DMF extract absorption. These results highlight the importance of
52 testing different solvents to investigate the structures and light absorption of BrC,

53 particularly for the low-volatility fraction potentially originating from non-combustion
54 sources.

55

56

57

58

59

60

61

62

63

64

65

66

67

68

69

70

71

72

73

74

75

76

77

78 **1 Introduction**

79 Besides black carbon (BC) and mineral dust, growing evidence shows that organic
80 carbon (OC) aerosols derived from various combustion sources (e.g., biofuel and fossil
81 fuel) and secondary processes (e.g., gas-phase oxidation, aqueous and in-cloud
82 processes) can absorb sunlight at short visible and UV wavelengths (Laskin et al., 2015;
83 Hems et al., 2021). The radiative forcing (RF) of the light-absorbing organic carbon,
84 also termed “brown carbon” (BrC), is not well quantified due to the lack of its emission
85 data, complex secondary formations, and large uncertainties in *in situ* BrC
86 measurements (Wang et al., 2014; Wang et al., 2018; Saleh, 2020). The imaginary part
87 of the refractive index (k) of BrC is required when modeling its influence on aerosols
88 direct RF, and is retrieved by the optical closure method combining online monitoring of
89 aerosol absorption and size distributions with Mie theory calculations (Lack et al., 2012;
90 Saleh et al., 2013; Saleh et al., 2014). However, several pre-assumptions must be made
91 on aerosol morphology (spherical Mie model) and mixing states of BC and organic
92 aerosols (OA), which might introduce large uncertainties in the estimation of k (Mack
93 et al., 2010; Xu et al., 2021).

94 To improve the understanding on chemical composition and light-absorbing
95 properties of BrC chromophores, organic matter (OM) in aerosols was isolated through
96 solvent extraction using water and/or methanol, followed by filtration and a series of
97 instrumental analysis (e.g., UV/Vis spectrometer, liquid chromatograph-mass
98 spectrometer; Chen and Bond, 2010; Liu et al., 2013; Lin et al., 2016). Referring to
99 existing studies, a larger fraction of the methanol extract absorption comes from water-
100 insoluble OM containing conjugated structures (Chen and Bond, 2010; Huang et al.,
101 2020); the light absorption of biomass burning OM is majorly contributed by large
102 molecules (MW > 500~1000 Da; Di Lorenzo and Young, 2016; Di Lorenzo et al., 2017)

103 and depends on burn conditions (Saleh et al., 2014); polycyclic aromatic hydrocarbons
104 (PAHs) and nitroaromatic compounds (NACs) are ubiquitous BrC chromophores in the
105 atmosphere (Huang et al., 2018; Wang et al., 2019), but the identified species only
106 explain a few percentages (< 10%) of total BrC absorption (Huang et al., 2018; Li et
107 al., 2020).

108 Methanol can extract > 90% OM from biomass burning (Chen and Bond, 2010;
109 Xie et al., 2017b), while the extraction efficiency (η , %) decreases to ~80% for ambient
110 organic aerosols (Xie et al., 2019b; Xie et al., 2022) possibly due to other sources
111 emitting large hydrophobic molecules and oligomerizations of small molecules during
112 the aging process (Cheng et al., 2021; Li et al., 2021). The light-absorbing properties
113 and structures of methanol-insoluble OC (MIOC) are still unknown. By comparing BrC
114 characterization results of offline and online methods, some studies conclude that the
115 MIOC dominates BrC absorption in source and ambient aerosols (Bai et al., 2020; Atwi
116 et al., 2022). However, the online-retrieval and offline-extraction methods are designed
117 based on different instrumentation and purposes, and the online method depends largely
118 on presumed and uncertain optical properties of BC (Wang et al., 2014). Given that the
119 solvent extract absorption is not converted to particulate absorption with Mie
120 calculations, solvent and pH effects are not accounted for, and BrC is not completely
121 dissolved in typical solvents (e.g., water and methanol), BrC absorption in particles and
122 solution can hardly be compared directly. To reveal the absorption and composition of
123 MIOC, it is necessary to find a new solvent or develop a new methodology to improve
124 OC extraction efficiency (Shetty et al., 2019).

125 In this work, a series of single solvents and solvent blends were tested for extraction
126 efficiencies of OC in ambient particulate matter with aerodynamic diameter < 2.5 μm
127 ($\text{PM}_{2.5}$), and the sample extract absorption of each solvent was compared. The solvent

128 or solvent mixture with the highest η value was applied to extract a matrix of collocated
129 PM_{2.5} samples followed by light absorption measurements. In our previous work, the
130 light absorption of methanol extracts of the same samples was measured, and source
131 apportionment was performed using organic molecular marker data (Xie et al., 2022).
132 By comparing with the study results in Xie et al. (2022), this study evaluated potential
133 underestimation of BrC absorption in methanol and its impacts on BrC source
134 attributions. These results suggest that different solvents should be used in future
135 investigations on the absorption, composition, sources, and formation pathways of low-
136 volatility BrC.

137 **2. Methods**

138 *2.1 Solvent selection*

139 Five solvents and solvent mixtures including water, methanol (MeOH),
140 MeOH/dichloromethane (MeOH/DCM, 1:1, v:v), MeOH/DCM (1:2, v:v),
141 tetrahydrofuran (THF), and N,N-dimethylformamide (DMF) were selected to extract
142 OC from identical PM_{2.5} samples to determine which solvent or solvent mixture has the
143 highest η value. Water and methanol are the most commonly used solvents to extract
144 BrC from source or ambient particles. Cheng et al. (2021) found that OC produced
145 through the combustion of toluene, isooctane, and cyclohexane were more soluble in
146 DCM than MeOH. Since a major part of BrC absorption is coming from unknown large
147 molecules (Di Lorenzo and Young, 2016; Di Lorenzo et al., 2017), polar aprotic
148 solvents THF and DMF were tested due to their high capacity for dissolving large
149 polymers. Except for water and MeOH, DCM and THF were rarely used to extract OC
150 for light absorption measurements (Cheng et al., 2021; Moschos et al. 2021), and DMF
151 has not ever been tested for extracting BrC in literature.

152 *2.2 Sampling*

153 **Sampling for solvent test.** To compare OC extraction efficiencies and extract
154 absorption of the five selected solvents and solvent mixtures, twenty-one ambient PM_{2.5}
155 samples were collected on the rooftop of a seven-story library building in Nanjing
156 University of Information Science and Technology (NUIST, 32.21°N, 118.71°E).
157 Details of the sampling site and equipment were provided by Yang et al. (2021). Two
158 identical mid-volume samplers (Sampler I and II; PM_{2.5}-PUF-300, Mingye
159 Environmental, China) equipped with 2.5 μm cut-point impactors were used for
160 ambient air sampling during day-time (8:00 a.m.–7:00 p.m.) and night-time (8:00 p.m.–
161 7:00 a.m. the next day), respectively, in December 2019. After the impactor, PM_{2.5} in
162 the air stream was collected on a pre-baked (550 °C, 4 h) quartz filter (20.3 cm ×12.6
163 cm, Munktell Filter AB, Sweden) at a flow rate of 300 L min⁻¹. PM_{2.5} filter and field
164 blank samples were sealed and stored at –20 °C before chemical analysis. Information
165 about PM_{2.5} samples for the solvent test is provided in Table S1 of supplementary
166 information.

167 **Ambient sampling for BrC analysis.** Details of the ambient sampling were described
168 in previous work (Qin et al., 2021; Yang et al., 2021; Xie et al., 2022). Briefly, Sampler
169 I and II were equipped with two quartz filters in series (quartz behind quartz, QBQ
170 method; Q_f and Q_b) followed by adsorbents. Collocated filter and adsorbent samples
171 were collected every sixth day during daytime and nighttime from 2018/09/28 to
172 2019/09/28. Field blank sampling was performed every 10th sample to address
173 contamination. Q_f samples loaded with PM_{2.5} were speciated and extracted for light
174 absorption measurements. The OC adsorbed on Q_b and its light absorption were
175 analyzed to determine positive sampling artifacts. The adsorbents in sampler I [a
176 polyurethane foam (PUF)/XAD-4 resin/PUF sandwich] and II (a PUF plug) were used
177 to collect gas-phase nonpolar and polar organic compounds, respectively. The

178 measurement results of gas- and particle-phase organic compounds were provided by
179 Gou et al. (2021) and Qin et al. (2021).

180 *2.3 Solvent test for light absorption and extraction efficiency*

181 An aliquot (~6 cm²) of each filter sample was extracted ultrasonically in 10 mL of
182 each solvent or solvent mixture (HPLC grade) for 30 min (one-time extraction
183 procedure, $N = 11$; Table S1). After filtration, the light absorbance (A_λ) of individual
184 solvent extracts was measured over 200–900 nm using a UV/Vis spectrometer (UV-
185 1900, Shimadzu Corporation, Japan), and was converted to light absorption coefficient
186 (Abs_λ , Mm⁻¹) by

$$187 \quad Abs_\lambda = (A_\lambda - A_{700}) \times \frac{V_l}{V_a \times L} \ln(10) \quad (1)$$

188 where A_{700} is subtracted to correct baseline drift, V_l (m³) is the air volume of the
189 extracted sample, L (0.01 m) is the optical path length, and $\ln(10)$ was multiplied to
190 transform Abs_λ from a common to a natural logarithm (Hecobian et al., 2010). To
191 understand if multiple extractions could draw out more BrC, a two-time extraction
192 procedure was applied for another 10 ambient PM_{2.5} samples in the same manner (Table
193 S1). The A_λ of the 1st and 2nd extractions (10 mL each) was measured separately for
194 Abs_λ calculations.

195 Prior to solvent extractions, the concentrations of OC and EC in each filter sample
196 were analyzed using a thermal-optical carbon analyzer (DRI, 2001A, Atmoslytic,
197 United States) following the IMPROVE-A protocol. OC and EC were converted to CO₂
198 step by step during two separate heating cycles [OC1 (140°C) – OC2 (280°C) – OC3
199 (480°C) – OC4 (580°C) in pure He, EC1 (580°C) – EC2 (740°C) – EC3 (840°C) in 98%
200 He/2% O₂], and the emitted CO₂ during each heating step was converted to CH₄ and
201 measured using a flame ionization detector (FID).

202 After extractions, filters extracted by MeOH, MeOH/DCM (1:1), MeOH/DCM
203 (1:2), and THF were air-dried in a fume hood and analyzed for residual OC (rOC, μg
204 m^{-3}) using the identical method. Filters extracted in water and DMF cannot be air-dried
205 in the short term due to the low volatility of solvents, and their rOC was measured after
206 baking at 100 °C for 2 h. The total amount of OC dissolved in water for each sample
207 was also measured as water-soluble OC (WSOC) by a total organic carbon analyzer
208 (TOC-L, Shimadzu, Japan; Yang et al., 2021). To examine if the baking process would
209 influence rOC measurements, the rOC of filters extracted in MeOH, MeOH/DCM
210 mixtures, and THF were also measured after the baking process and compared to those
211 determined after air dried. The pyrolytic carbon (PC) was used to correct for sample
212 charring and was determined when the filter transmittance or reflectance returned to its
213 initial value during the analysis (Schauer et al., 2003), but the formation of PC is very
214 scarce when analyzing extracted filters. In this study, solvent-extractable OC (SEOC,
215 $\mu\text{g m}^{-3}$) was determined by the difference in OC1–OC4 between pre- and post-
216 extraction samples. The extraction efficiency (η , %) of each solvent was expressed as

$$217 \quad \eta = \frac{\text{SEOC}}{\text{OC}} \times 100\% \quad (2)$$

218 Here, SEOC denotes WSOC when the solvent is water. For the ambient samples
219 extracted twice, rOC was measured only after the two-extraction procedure was
220 completed.

221 The solution mass absorption efficiency (MAE_λ , $\text{m}^2 \text{g}^{-1} \text{C}$) was calculated by
222 dividing Abs_λ by the concentration of SEOC

$$223 \quad \text{MAE}_\lambda = \frac{\text{Abs}_\lambda}{\text{SEOC}} \quad (3)$$

224 and the solution absorption Ångström exponent (Å), a parameter showing the
225 wavelength dependence of solvent extract absorption, was obtained from the regression

226 slope of $\lg(\text{Abs}_\lambda)$ versus $\lg(\lambda)$ over 300–550 nm.

227 The solvent effect is not uncommon when measuring aerosol extract absorbance in
228 difference solvents (Chen and Bond, 2010; Mo et al., 2017; Moschos et al., 2021), but
229 is rarely accounted for in previous studies. To evaluate the influence of solvent effects
230 on light absorption of different solvent extracts of the same sample, solutions of 4-
231 nitrophenol at 1.90 mg L^{-1} , 4-nitrocatechol at 1.84 mg L^{-1} , and 25-PAH mixtures (Table
232 S2) at 0.0080 mg L^{-1} and 0.024 mg L^{-1} (each species) in the five solvents and solvent
233 mixtures were made up for five times and analyzed for UV/Vis spectra. The absorbance
234 of PAH mixtures in water was not provided due to their low solubility.

235 *2.3 Measurements and analysis of ambient BrC absorption*

236 Collocated Q_f and Q_b samples were extracted using the solvent with the highest η
237 value once followed by light absorbance measurement. OC concentrations in Q_f and Q_b
238 samples were obtained from Yang et al. (2021), and SEOC values were estimated from
239 OC concentrations and the average η value determined in *section 2.1* for one-time
240 extraction. In this work, Q_b measurements were used to correct Abs_λ , MAE_λ , and \AA of
241 BrC in ambient $\text{PM}_{2.5}$ in the same manner as those for water and methanol extracts in
242 Xie et al. (2022)

$$243 \text{Artifact-corrected } \text{Abs}_\lambda = \text{Abs}_\lambda^{Q_f} - \text{Abs}_\lambda^{Q_b} \quad (4)$$

$$244 \text{Artifact-corrected } \text{MAE}_\lambda = \frac{\text{Abs}_\lambda^{Q_f} - \text{Abs}_\lambda^{Q_b}}{\text{SEOC}_{Q_f} - \text{OC}_{Q_b}} \quad (5)$$

245 where $\text{Abs}_\lambda^{Q_f}$ and $\text{Abs}_\lambda^{Q_b}$ are Abs_λ values of Q_f and Q_b samples, respectively; SEOC_{Q_f}
246 represents SEOC concentrations in Q_f samples; OC_{Q_b} denotes OC concentrations in Q_b
247 samples, assuming that OC in Q_b is completely dissolved (Xie et al., 2022). Artifact
248 corrected \AA were generated from the regression slope of $\lg(\text{Abs}_\lambda^{Q_f} - \text{Abs}_\lambda^{Q_b})$ versus \lg
249 (λ) over 300 – 550 nm. Artifact-corrected Abs_λ , MAE_λ , and \AA during each sampling

250 interval were determined by averaging each pair of collocated measurements. If one of
251 the two numbers in a pair is missed, the other number will be directly used for the
252 specific sampling interval. To compare with previous studies based on water and/or
253 methanol extraction methods, Abs_{λ} and MAE_{λ} at 365 nm were shown and discussed in
254 this work.

255 Pearson's correlation coefficient (r) was used to show how collocated
256 measurements of BrC in ambient $PM_{2.5}$ vary together. The coefficient of divergence
257 (COD) was calculated to indicate consistency between collocated measurements. The
258 relative uncertainty of BrC absorption derived from duplicate data was depicted using
259 the average relative percent difference (ARPD, %), which was used as the uncertainty
260 fraction for BrC measurements. Calculation methods of COD and ARPD are provided
261 in Text S1 of supplementary information. To examine the influence of potential BrC
262 underestimation based on the methanol extraction method on source apportionment,
263 positive matrix factorization (PMF) version 5.0 (U.S. Environmental Protection
264 Agency) was applied to attribute the light absorption of aerosol extracts in methanol
265 and solvent with the highest η to sources. The total concentration data ($Q_f + Q_b +$
266 adsorbent) of organic compounds have been used to apportion the light absorption of
267 MeOH-soluble OC to specific sources (Xie et al., 2022), so as to avoid the impacts of
268 gas-particle partitioning. In this work, the input particulate bulk components and total
269 organic molecular marker (OMM) data for PMF analysis were obtained from Xie et al.
270 (2022) and are summarized in Table S3. Four- to ten-factor solutions were tested to
271 retrieve a final factor number with the most physically interpretable base-case solution.
272 More information on input data preparation and the factor number determination are
273 provided in supplementary information (Text S2 and Table S4).

274 **3. Results and discussion**

275 3.1 Solvent test

276 3.1.1 Extraction efficiency of different solvents

277 The concentrations of OC and EC fractions in each sample prior to solvent
278 extractions are listed in Table S1. SEOC concentrations and extraction efficiencies of
279 individual solvents and solvent mixtures are detailed in Table 1. Generally, DMF
280 presented the highest extraction efficiency of total OC whenever filter samples were
281 extracted once ($89.0 \pm 7.96\%$) or twice ($95.6 \pm 3.67\%$), followed by MeOH (one-time
282 extraction $82.3 \pm 8.68\%$, two-time extraction $86.6 \pm 7.86\%$) and MeOH/DCM mixtures
283 ($\sim 75\%$, $\sim 85\%$). Although THF and DMF are frequently used to dissolve polymers (e.g.,
284 polystyrene) for characterization, THF had the lowest η values ($64.2 \pm 8.08\%$, $70.1 \pm$
285 8.01%) comparable to water ($66.7 \pm 8.58\%$, $69.9 \pm 5.88\%$). Compared with one-time
286 extraction, the extraction efficiencies of selected solvents were improved by a few
287 percent when filter samples were extracted twice, and η values of MeOH/DCM
288 mixtures became closer to those of MeOH (Table 1). These results showed that solvents
289 can reach more than 80% of their dissolving capacity with the one-time extraction, and
290 the ambient OC in Nanjing is more soluble in MeOH than in DCM.

291 From OC1 to OC4, the volatility of OC fractions is expected to decrease
292 continuously, and the molecules in OC fractions evolving at higher temperatures should
293 be larger than those in OC1 with similar functional groups. In Table 1, MeOH and
294 MeOH/DCM mixtures had comparable or even higher η values ($82.6 \pm 25.9\%$ – $97.9 \pm$
295 5.02%) of OC1 and OC2 than DMF ($88.8 \pm 4.98\%$ – $97.2 \pm 2.12\%$). But OC3 and OC4
296 accounted for more than 60% of OC concentrations, and DMF exhibited significant (p
297 < 0.05) larger η values than other solvents, indicating that DMF had stronger dissolving
298 capacity for large organic molecules than MeOH.

299 Concentrations of extracted OC fractions in MeOH, MeOH/DCM mixtures, and

300 THF based on the two methods for rOC measurements (*section 2.2*) are compared in
301 Figures S1 and S2. The total SEOC concentrations derived from the two methods are
302 compared in Figure S3. All the scatter data of SEOC fell along the 1:1 line with
303 significant correlations ($r > 0.85$, $p < 0.01$). Because the measurement uncertainty of
304 dominant species is lower than minor ones (Hyslop and White, 2008; Yang et al., 2021),
305 the slightly greater relative difference between the two methods for extractable OC1
306 was likely attributed to its low concentrations ($< 1 \mu\text{g m}^{-3}$; Tables 1 and S1). Thus,
307 baking extracted filters to dryness was expected to have little influence on SEOC
308 measurements, particularly for low-volatility OC fractions (OC2-OC4).

309 Although water dissolves less OC than MeOH, WSOC is intensively extracted and
310 analyzed for its composition and light absorption (Hecobian et al., 2010; Liu et al., 2013;
311 Washenfelder et al., 2015). WSOC can play a significant role in changing the radiative
312 and cloud-nucleating properties of atmospheric aerosols (Hallar et al., 2013; Taylor et
313 al., 2017). It also served as a proxy measurement for oxygenated (OOA) or secondary
314 organic aerosols (SOA) in some regions (Kondo et al., 2007; Weber et al., 2007). In
315 previous work, MeOH was commonly used as the most efficient solvent in extracting
316 OC from biomass burning ($\eta > 90\%$; Chen and Bond, 2010; Xie et al., 2017b) and
317 ambient particles ($\eta \sim 80\%$; Xie et al., 2019b; Xie et al., 2022). MeOH-insoluble OC
318 has rarely been investigated through direct solvent-extraction followed by instrumental
319 analysis. There is evidence showing that BrC absorption is associated mostly with large
320 molecular weight and extremely low-volatility species (Saleh et al., 2014; Di Lorenzo
321 and Young, 2016; Di Lorenzo et al., 2017). Compared with DMF, the lower capability
322 of MeOH in dissolving OC3 and OC4 would lead to an underestimation of BrC
323 absorption in atmospheric aerosols.

324 3.1.2 Light absorption of different solvent extracts

325 Table 2 shows the average Abs_{λ} and MAE_{λ} values of different solvent extracts at
326 365 and 550 nm. The Abs_{λ} and MAE_{λ} spectra of selected samples are illustrated in
327 Figure S4. Not including DMF, MeOH extracts exhibited the strongest light absorption.
328 Since MeOH can dissolve more OC3 and OC4 than DCM (Table 1), the Abs_{λ} and MAE_{λ}
329 of MeOH/DCM extracts decreased as the fraction of DCM increased in solvent
330 mixtures (Table 2 and Figure S4). Water and THF extracts had the smallest Abs_{λ} and
331 MAE_{λ} due to their low extraction efficiencies for low-volatility OC (OC2-OC4; Table
332 1). In comparison to MeOH extracts, $Abs_{365/550}$ and $MAE_{365/550}$ of DMF extracts were
333 at least more than 40% higher ($p < 0.05$). Given that the relative difference in extraction
334 efficiency of total OC between MeOH and DMF was less than 10% and DMF dissolved
335 more OC3 and OC4 than other solvents (Table 1), low-volatility OC should contain
336 stronger light-absorbing chromophores (Saleh et al., 2014) and its mass fraction might
337 determine the difference in BrC absorption across solvent extraction methods.
338 Moreover, the relative difference in Abs_{λ} and MAE_{λ} between MeOH and DMF extracts
339 increased with wavelength (Table 2 and Figure S4). This is because the light absorption
340 of DMF extracts that contain stronger BrC chromophores depends less on wavelengths
341 than other solvent extracts ($\bar{A} \sim 4.5$, Table 2). As shown in Figure S5, average \bar{A} and
342 $MAE_{365/550}$ values of individual solvent extracts in Table 2 are negatively correlated.

343 In this work, insoluble organic particles coming off the filter during sonication
344 might lead to overestimated SEOC concentrations and η values, and then the MAE_{λ} of
345 solvent extracts would be underestimated. Previous studies rarely considered the loss
346 of insoluble OC during the extraction process (Yan et al., 2020), of which the impact
347 on MAE_{λ} calculation was still inconclusive. But Abs_{λ} measurements would never be
348 influenced, as the light absorbance of solvent extracts was analyzed after filtration. In
349 Table 2, the second extraction only increases the average Abs_{365} and Abs_{550} values of

350 DMF extracts by 6.70% ($p = 0.78$) and 6.76% ($p = 0.77$), respectively. We suspected
351 that the difference in η values of DMF between one-time and two-time extraction
352 procedures was mainly ascribed to the detachment of insoluble OC particles.

353 In Figure S6, the absorbance spectra of 4-nitrophenol and 4-nitrocatechol in water
354 shift toward longer wavelengths compared to their MeOH solution. This is because
355 neutral and deprotonated forms of 4-nitrophenol and 4-nitrocatechol may have different
356 absorbance spectra, and these two compounds are deprotonated at $\text{pH} \approx 7$ (Lin et al.,
357 2015b, 2017). The strong light absorption of 4-nitrophenol and 4-nitrocatechol in DMF
358 at 450 nm was not observed in other solvents, and was likely caused by unknown
359 reactions. Then the solvent effect introduced by DMF might overestimate the light
360 absorption of low-molecular-weight (LMW) nitrophenol-like species at > 400 nm in
361 source or ambient aerosols. Evidence shows that BrC absorption is dominated by large
362 molecules with extremely low volatility (Saleh et al., 2014; Di Lorenzo and Young,
363 2016; Di Lorenzo et al., 2017), and LMW nitrophenol-like species have very low
364 contributions to particulate OM (e.g., $< 1\%$) and aerosol extract absorption (e.g., $< 10\%$)
365 (Mohr et al., 2013; Zhang et al., 2013; Teich et al., 2017; Xie et al., 2019a, 2020; Li et
366 al., 2020). The shapes of the light absorption spectra of aerosol extracts in DMF were
367 similar to other solvents (Figure S4) and PAH solutions (Figure S6g-1), and no elevation
368 in light absorption appeared at 400–500 nm. Thus, the overestimated absorption of
369 LMW nitrophenol-like species in DMF might not substantially impact the overall BrC
370 absorption of aerosol extracts. Furthermore, the absorbance of 4-nitrophenol and 4-
371 nitrocatechol in DMF at 365 nm (A_{365}) was lower than that in MeOH, and PAH
372 solutions showed very similar absorbance spectra across the five solvents (Figure S6g–
373 1 and Table S5). Considering that low-volatility OC fractions (e.g., OC3 and OC4) in
374 the ambient are less water soluble (Table 1) and have a high degree of conjugation

375 (Chen and Bond, 2010; Lin et al., 2014), their structures are probably featured by a
376 PAH skeleton. Therefore, the large difference in Abs_{365} between DMF and MeOH
377 extracts (Table 2) was primarily ascribed to the fact that DMF can dissolve more OC3
378 and OC4 than methanol (Table 1). However, we cannot rule out the impact of solvent
379 effects on the comparison of light absorption spectra between MeOH and DMF extracts
380 (Figure S4), and more work is warranted in identifying the structures more soluble in
381 DMF than in MeOH.

382 *3.2 Collocated measurements and temporal variability*

383 Abs_{365} values of collocated Q_f and Q_b extracts in DMF are summarized in Table S6.
384 No significant difference was observed (Q_f $p = 0.96$; Q_b $p = 0.42$) between the two
385 samplers. After Q_b corrections, Abs_{365} , MAE_{365} , and \dot{A} of DMF extractable OC ($Abs_{365,d}$,
386 $MAE_{365,d}$, and \dot{A}_d) in $PM_{2.5}$ were calculated by averaging each pair of duplicate Q_f - Q_b
387 data, and are compared with those of methanol extracts ($Abs_{365,m}$, $MAE_{365,m}$, and \dot{A}_m)
388 in Table 3. Figure 1 shows comparisons between collocated measurements of $Abs_{365,d}$,
389 $MAE_{365,d}$, and \dot{A}_d . Generally, all comparisons indicated good agreement with $COD <$
390 0.20 (0.094 – 0.15). $Abs_{365,d}$ and $MAE_{365,d}$ had comparable uncertainty fractions (ARPD,
391 22.7% and 24.5% , Figure 1) as $Abs_{365,m}$ and $MAE_{365,m}$ (28.4% and 28.8% ; Xie et al.,
392 2022). Since different primary combustion sources can have similar spectral
393 dependence for BrC absorption (Chen and Bond, 2010; Xie et al., 2017b; Xie et al.,
394 2018; Xie et al., 2019a), most \dot{A}_d data clustered on the identity line with much lower
395 variability than $Abs_{365,d}$ and $MAE_{365,d}$. As shown in Table 3, average $Abs_{365,d}$ and
396 $MAE_{365,d}$ values were 30.7% ($p < 0.01$) and 17.3% ($p < 0.05$) larger than average
397 $Abs_{365,m}$ and $MAE_{365,m}$. Because the k value of BrC in bulk solution is directly estimated
398 from Abs_λ or MAE_λ (Liu et al., 2013; Liu et al., 2016; Lu et al., 2015), the estimation
399 method needs to be revised when ambient BrC is extracted using DMF instead of

400 MeOH. Both $MAE_{365,d}$ and $MAE_{365,m}$ were negatively correlated ($p < 0.01$) with their
401 corresponding \hat{A} values (Figure S7), and the lower average \hat{A}_d (5.25 ± 0.64 , $p < 0.01$)
402 compared to \hat{A}_m (6.81 ± 1.64 ; Table 3) supports that more-absorbing BrC had less
403 spectral dependence than less-absorbing BrC.

404 Figure 2 compares the time series of Abs_{365} , MAE_{365} , and \hat{A} between the DMF and
405 MeOH extracts. Both DMF and MeOH extracts had significant ($p < 0.05$) higher
406 absorption at night-time than during the daytime due to the “photo-bleaching” effect
407 (Zhang et al., 2020; Xie et al., 2022). All the three parameters of DMF and MeOH
408 extracts exhibited consistency in winter (Figure 2) when biomass burning dominated
409 BrC absorption (Xie et al., 2022). While in later spring and summer (2019/05/15–
410 2019/08/01), average $Abs_{365,d}$ and $MAE_{365,d}$ values were more than two times greater
411 than the average $Abs_{365,m}$ and $MAE_{365,m}$. Many studies have identified a temporal
412 pattern of BrC absorption with winter maxima and summer minima based on
413 water/MeOH extraction methods (Lukács et al., 2007; Zhang et al., 2010; Du et al.,
414 2014; Zhu et al., 2018). Due to the low capability of water and MeOH in dissolving
415 large BrC molecules, BrC absorption and its temporal variations in these studies might
416 be biased. Moreover, the identification of BrC sources using receptor models is highly
417 dependent on the difference in the time series of input species (Dall'Osto et al., 2013).
418 Then, using DMF instead of MeOH for BrC extraction and measurements will lead to
419 distinct source apportionment results.

420 *3.3 Sources of DMF and MeOH Extractable BrC*

421 A final factor number of eight was determined based on the interpretability of
422 different base-case solutions (four to ten factors), the change in Q/Q_{exp} with factor
423 numbers, and robustness analysis (Text S2 and Table S4). Normalized factor profiles of
424 seven- to nine-factor solutions are compared in Figure S8. The seven-factor solution

425 failed to resolve the lubricating oil combustion factor characterized by hopanes and
426 steranes (Figure S8c). An unknown factor containing various source tracers related to
427 crustal dust (Ca^{2+} and Mg^{2+}), lubricating oil (hopanes and steranes), and soil microbiota
428 (sugar and sugar alcohols) was identified in the nine-factor solution (Figure S8i).
429 Median and mean values of input $\text{Abs}_{365,\text{d}}$, $\text{Abs}_{365,\text{m}}$, and bulk component concentrations
430 agreed well with PMF estimations (Table S7), and the strong correlations ($r = 0.86$ –
431 0.99) between observations and PMF estimations indicated that the eight-factor
432 solution simulated the time series of input species well. In comparison to Xie et al.
433 (2022), where Abs_{365} of MeOH and water extracts were apportioned to nine sources
434 using the same speciation data, this work lumped secondary nitrate and sulfate to the
435 same factor (termed “secondary inorganics”, Figure S8h), and the other seven factors
436 had similar factor profiles linked with biomass burning, non-combustion fossil,
437 lubricating oil combustion, coal combustion, dust resuspension, biogenic emission, and
438 isoprene oxidation. Interpretations of individual factors based on characteristic source
439 tracers and contribution time series were provided in previous work (Gou et al., 2021;
440 Xie et al., 2022).

441 The average relative contributions of the identified factors to $\text{Abs}_{365,\text{d}}$, $\text{Abs}_{365,\text{m}}$, and
442 bulk components are listed in Table S8. Consistent contribution distributions of $\text{Abs}_{365,\text{m}}$
443 were observed between Xie et al. (2022) and this study, indicating that the PMF results
444 were robust to the inclusion of $\text{Abs}_{365,\text{d}}$ data. Figure 3 compares the time series of factor
445 contributions to $\text{Abs}_{365,\text{d}}$ and $\text{Abs}_{365,\text{m}}$. ARPD and COD values between factor
446 contributions to $\text{Abs}_{365,\text{d}}$ and $\text{Abs}_{365,\text{m}}$ and the absolute difference are exhibited in Figure
447 S9. $\text{Abs}_{365,\text{d}}$ and $\text{Abs}_{365,\text{m}}$ had comparable contributions from biomass burning,
448 lubricating oil combustion, and coal combustion (Figure 3a, c, d). The small COD
449 values of these three factors (0.0041–0.17) indicated no significant divergence. The

450 biogenic emission and isoprene oxidation factors exhibited complete difference (ARPD
451 = 200%, COD = 1; Figure S9f, g) as they had no contribution to Abs_{365,m}. Among the
452 eight factors, the non-combustion fossil, dust resuspension, and isoprene oxidation
453 factors had the largest median difference in factor contributions to Abs_{365,d} and Abs_{365,m}
454 (0.63–0.67 Mm⁻¹) with substantial heterogeneity (COD > 0.20), followed by the
455 secondary inorganics factor (0.20 Mm⁻¹, COD = 0.41). The temporal variations of the
456 absolute difference shown in Figure S9 are identical to the contributions of individual
457 factors to Abs_{365,d} or Abs_{365,m} (Figure 3).

458 The non-combustion fossil factor represents unburned fossil-fuel emissions (e.g.,
459 petroleum products), which contain substantial large organic molecules (e.g., high MW
460 PAHs; Simoneit and Fetzer, 1996; Mi et al., 2000). This might explain why the non-
461 combustion fossil factor contributed more Abs_{365,d} than Abs_{365,m} all over the year
462 (Figure S9b). Dust resuspension and isoprene oxidation factors show prominent
463 contributions to Abs_{365,d} in spring and summer, respectively (Figure 3e, g). The dust
464 resuspension factor had the highest average contributions to both crustal materials (Ca²⁺
465 and Mg²⁺) and carbonaceous species (OC and EC; Table S8 and Figure S8), and was
466 considered a mixed source of crustal dust and motor vehicle emissions (Yu et al., 2020;
467 Xie et al., 2022). Besides the influences from primary emissions, aging processes of
468 organic components in dust aerosols can induce the formation of BrC through iron-
469 catalyzed polymerization (Link et al., 2020; Al-Abadleh, 2021; Chin et al., 2021). It
470 was demonstrated that the isoprene-derived polymerization products through aerosol-
471 phase reactions are light-absorbing chromophores (Lin et al., 2014; Nakayama et al.,
472 2015). This might explain the elevated difference between Abs_{365,d} and Abs_{365,m}
473 contributions of the isoprene oxidation factor in summer (Figure S9g). The biogenic
474 emission factor was characterized by tracers related to microbiota activities (sugar and

475 sugar alcohols) and decomposition of high plant materials (odd-numbered alkanes) in
476 soil (Rogge et al., 1993; Simoneit et al., 2004), and had negligible contributions (< 0.1%)
477 to Abs_{365,d} and Abs_{365,m}. Evidence shows that secondary BrC can be generated through
478 gas-phase reactions of anthropogenic volatile organic compounds with NO_x
479 (Nakayama et al., 2010; Liu et al., 2016; Xie et al., 2017a), aqueous reactions of SOA
480 with reduced nitrogen-containing species (e.g., NH₄⁺; Updyke et al., 2012; Powelson et
481 al., 2014; Lin et al., 2015a), and evaporation of water from droplets in the atmosphere
482 containing soluble organics (Nguyen et al., 2012; Kasthuriarachchi et al., 2020). These
483 processes can also lead to the formation of low-volatility oligomers (Nguyen et al.,
484 2012; Song et al., 2013), and their contributions might be lumped into the secondary
485 inorganics factor due to the lack of OMMs. According to these results, one possible
486 explanation for the difference in time series between Abs_{365,d} and Abs_{365,m} (Figure 2) is
487 that large BrC molecules from unburned fossil fuels and atmospheric processes are less
488 soluble in MeOH than in DMF.

489 **4. Conclusions and implications**

490 Comparisons of extraction efficiencies and light absorption of ambient aerosol
491 extracts across selected solvents and solvent mixtures indicate that MeOH may
492 sometimes be replaced with DMF for measuring BrC absorption, as low-volatility OC
493 fractions containing strong chromophores are less soluble in MeOH than in DMF.
494 Existing modeling studies on the radiative forcing of BrC (Feng et al., 2013; Wang et
495 al., 2014; Zhang et al., 2020) often retrieved or estimated its optical properties from
496 laboratory or ambient measurements based on water/methanol extraction methods
497 (Chen and Bond, 2010; Hecobian et al., 2010; Liu et al., 2013; Zhang et al., 2013), and
498 had a potential to underestimate the contribution of BrC to total aerosol absorption.
499 However, the influence of the solvent effect was not accounted for in this work when

500 comparing the light absorption of different solvent extracts. The difference between
501 MeOH and DMF extract absorption might change with the time and location due to the
502 variations in BrC sources. The results of this work also imply the necessity of applying
503 different solvents or combinations of solvents with broad polarity and dissolving
504 capability to study BrC composition and absorption, particularly for low-volatility
505 fractions.

506 Although light-absorbing properties of DMF and MeOH extracts had good
507 agreement in cold periods, when biomass and coal burning sources dominated BrC
508 emissions, their distinct time series in spring and summer implies that the contributions
509 of certain BrC sources were underestimated or missed when the MeOH extraction
510 method was used. Source apportionment results of Abs_{365,d} and Abs_{365,m} based on
511 organic molecular marker data indicated that large and methanol insoluble BrC
512 molecules are likely coming from unburned fossil fuels and polymerization of aerosol
513 organics. Laboratory studies have observed the polymerization process through
514 heterogeneous reactions of several precursors (e.g., catechol; Lin et al., 2014; Link et
515 al., 2020), but the structures and light-absorbing properties of potential polymerization
516 products in ambient aerosols (Figure 3e, g) are less understood and warrant further
517 study.

518

519 ***Data availability***

520 Data used in the writing of this paper is available at the Harvard Dataverse
521 (<https://doi.org/10.7910/DVN/CGHPXB>, Xu et al., 2022)

522

523 ***Author contributions***

524 MX designed the research. ZX, WF, YW, and HY performed laboratory experiments.

525 ZX, WF, and MX analyzed the data. ZX and MX wrote the paper with significant
526 contributions from YW and HL.

527

528 *Competing interests*

529 The authors declare that they have no conflict of interest.

530

531 *Acknowledgments*

532 This work was supported by the National Natural Science Foundation of China
533 (NSFC, 42177211, 41701551).

534

535 **References**

- 536 Al-Abadleh, H. A.: Aging of atmospheric aerosols and the role of iron in catalyzing brown carbon
537 formation, *Environ. Sci.: Atmos.*, 1, 297-345, 10.1039/D1EA00038A, 2021.
- 538 Atwi, K., Cheng, Z., El Hajj, O., Perrie, C., and Saleh, R.: A dominant contribution to light absorption
539 by methanol-insoluble brown carbon produced in the combustion of biomass fuels typically
540 consumed in wildland fires in the United States, *Environ. Sci.: Atmos.*, 10.1039/D1EA00065A, 2022.
- 541 Bai, Z., Zhang, L., Cheng, Y., Zhang, W., Mao, J., Chen, H., Li, L., Wang, L., and Chen, J.:
542 Water/methanol-insoluble brown carbon can dominate aerosol-enhanced light absorption in port
543 cities, *Environ. Sci. Technol.*, 54, 14889-14898, 10.1021/acs.est.0c03844, 2020.
- 544 Chen, Y., and Bond, T. C.: Light absorption by organic carbon from wood combustion, *Atmos. Chem.*
545 *Phys.*, 10, 1773-1787, 10.5194/acp-10-1773-2010, 2010.
- 546 Cheng, Z., Atwi, K., Hajj, O. E., Ijeli, I., Fischer, D. A., Smith, G., and Saleh, R.: Discrepancies between
547 brown carbon light-absorption properties retrieved from online and offline measurements, *Aerosol*
548 *Sci. Technol.*, 55, 92-103, 10.1080/02786826.2020.1820940, 2021.
- 549 Chin, H., Hopstock, K. S., Fleming, L. T., Nizkorodov, S. A., and Al-Abadleh, H. A.: Effect of aromatic
550 ring substituents on the ability of catechol to produce brown carbon in iron(iii)-catalyzed reactions,
551 *Environ. Sci.: Atmos.*, 1, 64-78, 10.1039/D0EA00007H, 2021.
- 552 Dall'Osto, M., Querol, X., Amato, F., Karanasiou, A., Lucarelli, F., Nava, S., Calzolari, G., and Chiari,
553 M.: Hourly elemental concentrations in PM_{2.5} aerosols sampled simultaneously at urban
554 background and road site during SAPUSS – diurnal variations and PMF receptor modelling, *Atmos.*
555 *Chem. Phys.*, 13, 4375-4392, 10.5194/acp-13-4375-2013, 2013.
- 556 Di Lorenzo, R. A., and Young, C. J.: Size separation method for absorption characterization in brown
557 carbon: Application to an aged biomass burning sample, *Geophys. Res. Lett.*, 43, 458-465,
558 10.1002/2015gl066954, 2016.
- 559 Di Lorenzo, R. A., Washenfelder, R. A., Attwood, A. R., Guo, H., Xu, L., Ng, N. L., Weber, R. J.,
560 Baumann, K., Edgerton, E., and Young, C. J.: Molecular-size-separated brown carbon absorption for
561 biomass-burning aerosol at multiple field sites, *Environ. Sci. Technol.*, 51, 3128-3137,
562 10.1021/acs.est.6b06160, 2017.
- 563 Du, Z., He, K., Cheng, Y., Duan, F., Ma, Y., Liu, J., Zhang, X., Zheng, M., and Weber, R.: A yearlong
564 study of water-soluble organic carbon in Beijing I: Sources and its primary vs. secondary nature,
565 *Atmos. Environ.*, 92, 514-521, <https://doi.org/10.1016/j.atmosenv.2014.04.060>, 2014.
- 566 Feng, Y., Ramanathan, V., and Kotamarthi, V. R.: Brown carbon: a significant atmospheric absorber of
567 solar radiation? *Atmos. Chem. Phys.*, 13, 8607-8621, 10.5194/acp-13-8607-2013, 2013.
- 568 Gou, Y., Qin, C., Liao, H., and Xie, M.: Measurements, gas/particle partitioning, and sources of nonpolar

569 organic molecular markers at a suburban site in the west Yangtze River Delta, China, *J. Geophys.*
570 *Res. Atmos.*, 126, e2020JD034080, <https://doi.org/10.1029/2020JD034080>, 2021.

571 Hallar, A. G., Lowenthal, D. H., Clegg, S. L., Samburova, V., Taylor, N., Mazzoleni, L. R., Zielinska, B.
572 K., Kristensen, T. B., Chirokova, G., McCubbin, I. B., Dodson, C., and Collins, D.: Chemical and
573 hygroscopic properties of aerosol organics at Storm Peak Laboratory, *J. Geophys. Res. Atmos.*, 118,
574 4767-4779, <https://doi.org/10.1002/jgrd.50373>, 2013.

575 Hecobian, A., Zhang, X., Zheng, M., Frank, N., Edgerton, E. S., and Weber, R. J.: Water-Soluble Organic
576 Aerosol material and the light-absorption characteristics of aqueous extracts measured over the
577 Southeastern United States, *Atmos. Chem. Phys.*, 10, 5965-5977, 10.5194/acp-10-5965-2010, 2010.

578 Hems, R. F., Schnitzler, E. G., Liu-Kang, C., Cappa, C. D., and Abbatt, J. P. D.: Aging of atmospheric
579 brown carbon aerosol, *ACS Earth Space Chem.*, 5, 722-748, 10.1021/acsearthspacechem.0c00346,
580 2021.

581 Huang, R.-J., Yang, L., Cao, J., Chen, Y., Chen, Q., Li, Y., Duan, J., Zhu, C., Dai, W., Wang, K., Lin, C.,
582 Ni, H., Corbin, J. C., Wu, Y., Zhang, R., Tie, X., Hoffmann, T., O'Dowd, C., and Dusek, U.: Brown
583 carbon aerosol in urban Xi'an, northwest China: The composition and light absorption properties,
584 *Environ. Sci. Technol.*, 52, 6825-6833, 10.1021/acs.est.8b02386, 2018.

585 Huang, R.-J., Yang, L., Shen, J., Yuan, W., Gong, Y., Guo, J., Cao, W., Duan, J., Ni, H., Zhu, C., Dai, W.,
586 Li, Y., Chen, Y., Chen, Q., Wu, Y., Zhang, R., Dusek, U., O'Dowd, C., and Hoffmann, T.: Water-
587 insoluble organics dominate brown carbon in wintertime urban aerosol of China: Chemical
588 characteristics and optical properties, *Environ. Sci. Technol.*, 54, 7836-7847,
589 10.1021/acs.est.0c01149, 2020.

590 Hyslop, N. P., and White, W. H.: An evaluation of interagency monitoring of protected visual
591 environments (IMPROVE) collocated precision and uncertainty estimates, *Atmos. Environ.*, 42,
592 2691-2705, <https://doi.org/10.1016/j.atmosenv.2007.06.053>, 2008.

593 Kasthuriarachchi, N. Y., Rivellini, L.-H., Chen, X., Li, Y. J., and Lee, A. K. Y.: Effect of relative humidity
594 on secondary brown carbon formation in aqueous droplets, *Environ. Sci. Technol.*, 54, 13207-13216,
595 10.1021/acs.est.0c01239, 2020.

596 Kondo, Y., Miyazaki, Y., Takegawa, N., Miyakawa, T., Weber, R. J., Jimenez, J. L., Zhang, Q., and
597 Worsnop, D. R.: Oxygenated and water-soluble organic aerosols in Tokyo, *J. Geophys. Res. Atmos.*,
598 112, D01203, 10.1029/2006jd007056, 2007.

599 Lack, D. A., Langridge, J. M., Bahreini, R., Cappa, C. D., Middlebrook, A. M., and Schwarz, J. P.: Brown
600 carbon and internal mixing in biomass burning particles, *Proc. Natl. Acad. Sci. U.S.A.*, 109, 14802-
601 14807, 10.1073/pnas.1206575109, 2012.

602 Laskin, A., Laskin, J., and Nizkorodov, S. A.: Chemistry of atmospheric brown carbon, *Chem. Rev.*, 115,
603 4335-4382, 10.1021/cr5006167, 2015.

604 Li, X., Yang, Y., Liu, S., Zhao, Q., Wang, G., and Wang, Y.: Light absorption properties of brown carbon
605 (BrC) in autumn and winter in Beijing: Composition, formation and contribution of nitrated aromatic
606 compounds, *Atmos. Environ.*, 223, 117289, <https://doi.org/10.1016/j.atmosenv.2020.117289>, 2020.

607 Li, Y., Ji, Y., Zhao, J., Wang, Y., Shi, Q., Peng, J., Wang, Y., Wang, C., Zhang, F., Wang, Y., Seinfeld, J.
608 H., and Zhang, R.: Unexpected oligomerization of small α -dicarbonyls for secondary organic aerosol
609 and brown carbon formation, *Environ. Sci. Technol.*, 55, 4430-4439, 10.1021/acs.est.0c08066, 2021.

610 Lin, P., Laskin, J., Nizkorodov, S. A., and Laskin, A.: Revealing brown carbon chromophores produced
611 in reactions of methylglyoxal with ammonium sulfate, *Environ. Sci. Technol.*, 49, 14257-14266,
612 10.1021/acs.est.5b03608, 2015a

613 Lin, P., Liu, J. M., Shilling, J. E., Kathmann, S. M., Laskin, J., and Laskin, A.: Molecular characterization
614 of brown carbon (BrC) chromophores in secondary organic aerosol generated from photo-oxidation
615 of toluene, *Phys. Chem. Chem. Phys.*, 17, 23312-23325, 10.1039/c5cp02563j, 2015b.

616 Lin, P., Bluvshstein, N., Rudich, Y., Nizkorodov, S. A., Laskin, J., and Laskin, A.: Molecular chemistry of
617 atmospheric brown carbon inferred from a nationwide biomass burning event, *Environ. Sci. Technol.*,
618 51, 11561-11570, 10.1021/acs.est.7b02276, 2017.

619 Lin, P., Aiona, P. K., Li, Y., Shiraiwa, M., Laskin, J., Nizkorodov, S. A., and Laskin, A.: Molecular
620 characterization of brown carbon in biomass burning aerosol particles, *Environ. Sci. Technol.*, 50,
621 11815-11824, 10.1021/acs.est.6b03024, 2016.

622 Lin, Y.-H., Budisulistiorini, S. H., Chu, K., Siejack, R. A., Zhang, H., Riva, M., Zhang, Z., Gold, A.,
623 Kautzman, K. E., and Surratt, J. D.: Light-absorbing oligomer formation in secondary organic
624 aerosol from reactive uptake of isoprene epoxydiols, *Environ. Sci. Technol.*, 48, 12012-12021,
625 10.1021/es503142b, 2014.

626 Link, N., Removski, N., Yun, J., Fleming, L. T., Nizkorodov, S. A., Bertram, A. K., and Al-Abadleh, H.
627 A.: Dust-catalyzed oxidative polymerization of catechol and its impacts on ice nucleation efficiency

628 and optical properties, *ACS Earth Space Chem.*, 4, 1127-1139, 10.1021/acsearthspacechem.0c00107,
629 2020.

630 Liu, J., Bergin, M., Guo, H., King, L., Kotra, N., Edgerton, E., and Weber, R. J.: Size-resolved
631 measurements of brown carbon in water and methanol extracts and estimates of their contribution to
632 ambient fine-particle light absorption, *Atmos. Chem. Phys.*, 13, 12389-12404, 10.5194/acp-13-
633 12389-2013, 2013.

634 Liu, J., Lin, P., Laskin, A., Laskin, J., Kathmann, S. M., Wise, M., Caylor, R., Imholt, F., Selimovic, V.,
635 and Shilling, J. E.: Optical properties and aging of light-absorbing secondary organic aerosol, *Atmos.*
636 *Chem. Phys.*, 16, 12815-12827, 10.5194/acp-16-12815-2016, 2016.

637 Lu, Z., Streets, D. G., Winijkul, E., Yan, F., Chen, Y., Bond, T. C., Feng, Y., Dubey, M. K., Liu, S., Pinto,
638 J. P., and Carmichael, G. R.: Light absorption properties and radiative effects of primary organic
639 aerosol emissions, *Environ. Sci. Technol.*, 49, 4868-4877, 10.1021/acs.est.5b00211, 2015.

640 Lukács, H., Gelencsér, A., Hammer, S., Puxbaum, H., Pio, C., Legrand, M., Kasper-Giebl, A., Handler,
641 M., Limbeck, A., Simpson, D., and Preunkert, S.: Seasonal trends and possible sources of brown
642 carbon based on 2-year aerosol measurements at six sites in Europe, *J. Geophys. Res. Atmos.*, 112,
643 <https://doi.org/10.1029/2006JD008151>, 2007.

644 Mack, L. A., Levin, E. J. T., Kreidenweis, S. M., Obrist, D., Moosmüller, H., Lewis, K. A., Arnott, W. P.,
645 McMeeking, G. R., Sullivan, A. P., Wold, C. E., Hao, W. M., Collett Jr, J. L., and Malm, W. C.:
646 Optical closure experiments for biomass smoke aerosols, *Atmos. Chem. Phys.*, 10, 9017-9026,
647 10.5194/acp-10-9017-2010, 2010.

648 Mo, Y., Li, J., Liu, J., Zhong, G., Cheng, Z., Tian, C., Chen, Y., and Zhang, G.: The influence of solvent
649 and pH on determination of the light absorption properties of water-soluble brown carbon, *Atmos.*
650 *Environ.*, 161, 90-98, <https://doi.org/10.1016/j.atmosenv.2017.04.037>, 2017.

651 Mohr, C., Lopez-Hilfiker, F. D., Zotter, P., Prévôt, A. S. H., Xu, L., Ng, N. L., Herndon, S. C., Williams,
652 L. R., Franklin, J. P., Zahniser, M. S., Worsnop, D. R., Knighton, W. B., Aiken, A. C., Gorkowski,
653 K. J., Dubey, M. K., Allan, J. D., and Thornton, J. A.: Contribution of nitrated phenols to wood
654 burning brown carbon light absorption in Detling, United Kingdom during winter time, *Environ. Sci.*
655 *Technol.*, 47, 6316-6324, 10.1021/es400683v, 2013.

656 Moschos, V., Gysel-Beer, M., Modini, R. L., Corbin, J. C., Massabò, D., Costa, C., Danelli, S. G.,
657 Vlachou, A., Daellenbach, K. R., Szidat, S., Prati, P., Prévôt, A. S. H., Baltensperger, U., and El
658 Haddad, I.: Source-specific light absorption by carbonaceous components in the complex aerosol
659 matrix from yearly filter-based measurements, *Atmos. Chem. Phys.*, 21, 12809-12833, 10.5194/acp-
660 21-12809-2021, 2021.

661 Mi, H.-H., Lee, W.-J., Chen, C.-B., Yang, H.-H., and Wu, S.-J.: Effect of fuel aromatic content on PAH
662 emission from a heavy-duty diesel engine, *Chemosphere*, 41, 1783-1790,
663 [https://doi.org/10.1016/S0045-6535\(00\)00043-6](https://doi.org/10.1016/S0045-6535(00)00043-6), 2000.

664 Nakayama, T., Matsumi, Y., Sato, K., Imamura, T., Yamazaki, A., and Uchiyama, A.: Laboratory studies
665 on optical properties of secondary organic aerosols generated during the photooxidation of toluene
666 and the ozonolysis of α -pinene, *J. Geophys. Res. Atmos.*, 115, D24204, 10.1029/2010jd014387,
667 2010.

668 Nakayama, T., Sato, K., Tsuge, M., Imamura, T., and Matsumi, Y.: Complex refractive index of secondary
669 organic aerosol generated from isoprene/NO_x photooxidation in the presence and absence of SO₂,
670 *J. Geophys. Res. Atmos.*, 120, 7777-7787, <https://doi.org/10.1002/2015JD023522>, 2015.

671 Nguyen, T. B., Lee, P. B., Updyke, K. M., Bones, D. L., Laskin, J., Laskin, A., and Nizkorodov, S. A.:
672 Formation of nitrogen- and sulfur-containing light-absorbing compounds accelerated by evaporation
673 of water from secondary organic aerosols, *J. Geophys. Res. Atmos.*, 117, D01207,
674 10.1029/2011jd016944, 2012.

675 Powelson, M. H., Espelien, B. M., Hawkins, L. N., Galloway, M. M., and De Haan, D. O.: Brown carbon
676 formation by aqueous-phase carbonyl compound reactions with amines and ammonium sulfate,
677 *Environ. Sci. Technol.*, 48, 985-993, 10.1021/es4038325, 2014.

678 Qin, C., Gou, Y., Wang, Y., Mao, Y., Liao, H., Wang, Q., and Xie, M.: Gas-particle partitioning of polyol
679 tracers at a suburban site in Nanjing, east China: increased partitioning to the particle phase, *Atmos.*
680 *Chem. Phys.*, 21, 12141-12153, 10.5194/acp-21-12141-2021, 2021.

681 Rogge, W. F., Hildemann, L. M., Mazurek, M. A., Cass, G. R., and Simoneit, B. R. T.: Sources of fine
682 organic aerosol .4. Particulate abrasion products from leaf surfaces of urban plants, *Environ. Sci.*
683 *Technol.*, 27, 2700-2711, 10.1021/es00049a008, 1993.

684 Saleh, R., Hennigan, C. J., McMeeking, G. R., Chuang, W. K., Robinson, E. S., Coe, H., Donahue, N.
685 M., and Robinson, A. L.: Absorptivity of brown carbon in fresh and photo-chemically aged biomass-
686 burning emissions, *Atmos. Chem. Phys.*, 13, 7683-7693, 10.5194/acp-13-7683-2013, 2013.

687 Saleh, R., Robinson, E. S., Tkacik, D. S., Ahern, A. T., Liu, S., Aiken, A. C., Sullivan, R. C., Presto, A.
688 A., Dubey, M. K., Yokelson, R. J., Donahue, N. M., and Robinson, A. L.: Brownness of organics in
689 aerosols from biomass burning linked to their black carbon content, *Nat. Geosci.*, 7, 647-650,
690 <https://doi.org/10.1038/ngeo2220>, 2014.

691 Saleh, R.: From measurements to models: Toward accurate representation of brown carbon in climate
692 calculations, *Curr. Pollut. Rep.*, 6, 90-104, 10.1007/s40726-020-00139-3, 2020.

693 Schauer, J. J., Mader, B. T., Deminter, J. T., Heidemann, G., Bae, M. S., Seinfeld, J. H., Flagan, R. C.,
694 Cary, R. A., Smith, D., Huebert, B. J., Bertram, T., Howell, S., Kline, J. T., Quinn, P., Bates, T.,
695 Turpin, B., Lim, H. J., Yu, J. Z., Yang, H., and Keywood, M. D.: ACE-Asia intercomparison of a
696 thermal-optical method for the determination of particle-phase organic and elemental carbon,
697 *Environ. Sci. Technol.*, 37, 993-1001, 10.1021/es020622f, 2003.

698 Shetty, N. J., Pandey, A., Baker, S., Hao, W. M., and Chakrabarty, R. K.: Measuring light absorption by
699 freshly emitted organic aerosols: Optical artifacts in traditional solvent-extraction-based methods,
700 *Atmos. Chem. Phys.*, 19, 8817-8830, 10.5194/acp-19-8817-2019, 2019.

701 Simoneit, B. R. T., and Fetzer, J. C.: High molecular weight polycyclic aromatic hydrocarbons in
702 hydrothermal petroleum from the Gulf of California and Northeast Pacific Ocean, *Org. Geochem.*,
703 24, 1065-1077, [https://doi.org/10.1016/S0146-6380\(96\)00081-2](https://doi.org/10.1016/S0146-6380(96)00081-2), 1996.

704 Simoneit, B. R. T., Elias, V. O., Kobayashi, M., Kawamura, K., Rushdi, A. I., Medeiros, P. M., Rogge,
705 W. F., and Didyk, B. M.: Sugars dominant water-soluble organic compounds in soils and
706 characterization as tracers in atmospheric particulate matter, *Environ. Sci. Technol.*, 38, 5939-5949,
707 10.1021/es0403099, 2004.

708 Song, C., Gyawali, M., Zaveri, R. A., Shilling, J. E., and Arnott, W. P.: Light absorption by secondary
709 organic aerosol from α -pinene: Effects of oxidants, seed aerosol acidity, and relative humidity, *J.*
710 *Geophys. Res. Atmos.*, 118, 11,741-711,749, 10.1002/jgrd.50767, 2013.

711 Taylor, N. F., Collins, D. R., Lowenthal, D. H., McCubbin, I. B., Hallar, A. G., Samburova, V., Zielinska,
712 B., Kumar, N., and Mazzoleni, L. R.: Hygroscopic growth of water soluble organic carbon isolated
713 from atmospheric aerosol collected at US national parks and Storm Peak Laboratory, *Atmos. Chem.*
714 *Phys.*, 17, 2555-2571, 10.5194/acp-17-2555-2017, 2017.

715 Teich, M., van Pinxteren, D., Wang, M., Kecorius, S., Wang, Z., Müller, T., Močnik, G., and Herrmann,
716 H.: Contributions of nitrated aromatic compounds to the light absorption of water-soluble and
717 particulate brown carbon in different atmospheric environments in Germany and China, *Atmos.*
718 *Chem. Phys.*, 17, 1653-1672, 10.5194/acp-17-1653-2017, 2017.

719 Updyke, K. M., Nguyen, T. B., and Nizkorodov, S. A.: Formation of brown carbon via reactions of
720 ammonia with secondary organic aerosols from biogenic and anthropogenic precursors, *Atmos.*
721 *Environ.*, 63, 22-31, <https://doi.org/10.1016/j.atmosenv.2012.09.012>, 2012.

722 Wang, X., Heald, C. L., Ridley, D. A., Schwarz, J. P., Spackman, J. R., Perring, A. E., Coe, H., Liu, D.,
723 and Clarke, A. D.: Exploiting simultaneous observational constraints on mass and absorption to
724 estimate the global direct radiative forcing of black carbon and brown carbon, *Atmos. Chem. Phys.*,
725 14, 10989-11010, 10.5194/acp-14-10989-2014, 2014.

726 Wang, X., Heald, C. L., Liu, J., Weber, R. J., Campuzano-Jost, P., Jimenez, J. L., Schwarz, J. P., and
727 Perring, A. E.: Exploring the observational constraints on the simulation of brown carbon, *Atmos.*
728 *Chem. Phys.*, 18, 635-653, 10.5194/acp-18-635-2018, 2018.

729 Wang, Y., Hu, M., Wang, Y., Zheng, J., Shang, D., Yang, Y., Liu, Y., Li, X., Tang, R., Zhu, W., Du, Z.,
730 Wu, Y., Guo, S., Wu, Z., Lou, S., Hallquist, M., and Yu, J. Z.: The formation of nitro-aromatic
731 compounds under high NO_x and anthropogenic VOC conditions in urban Beijing, China, *Atmos.*
732 *Chem. Phys.*, 19, 7649-7665, 10.5194/acp-19-7649-2019, 2019.

733 Washenfelder, R. A., Attwood, A. R., Brock, C. A., Guo, H., Xu, L., Weber, R. J., Ng, N. L., Allen, H.
734 M., Ayres, B. R., Baumann, K., Cohen, R. C., Draper, D. C., Duffey, K. C., Edgerton, E., Fry, J. L.,
735 Hu, W. W., Jimenez, J. L., Palm, B. B., Romer, P., Stone, E. A., Wooldridge, P. J., and Brown, S. S.:
736 Biomass burning dominates brown carbon absorption in the rural southeastern United States,
737 *Geophys. Res. Lett.*, 42, 653-664, 10.1002/2014gl062444, 2015.

738 Weber, R. J., Sullivan, A. P., Peltier, R. E., Russell, A., Yan, B., Zheng, M., de Gouw, J., Warneke, C.,
739 Brock, C., Holloway, J. S., Atlas, E. L., and Edgerton, E.: A study of secondary organic aerosol
740 formation in the anthropogenic-influenced southeastern United States, *J. Geophys. Res. Atmos.*, 112,
741 D13302, 10.1029/2007jd008408, 2007.

742 Xie, M., Chen, X., Hays, M. D., Lewandowski, M., Offenberg, J., Kleindienst, T. E., and Holder, A. L.:
743 Light absorption of secondary organic aerosol: Composition and contribution of nitroaromatic
744 compounds, *Environ. Sci. Technol.*, 51, 11607-11616, 10.1021/acs.est.7b03263, 2017a.

745 Xie, M., Hays, M. D., and Holder, A. L.: Light-absorbing organic carbon from prescribed and laboratory

746 biomass burning and gasoline vehicle emissions, *Sci. Rep.*, 7, 7318, 10.1038/s41598-017-06981-8,
747 2017b.

748 Xie, M., Shen, G., Holder, A. L., Hays, M. D., and Jetter, J. J.: Light absorption of organic carbon emitted
749 from burning wood, charcoal, and kerosene in household cookstoves, *Environ. Pollut.*, 240, 60-67,
750 <https://doi.org/10.1016/j.envpol.2018.04.085>, 2018.

751 Xie, M., Chen, X., Hays, M. D., and Holder, A. L.: Composition and light absorption of N-containing
752 aromatic compounds in organic aerosols from laboratory biomass burning, *Atmos. Chem. Phys.*, 19,
753 2899-2915, 10.5194/acp-19-2899-2019, 2019a.

754 Xie, M., Chen, X., Holder, A. L., Hays, M. D., Lewandowski, M., Offenberg, J. H., Kleindienst, T. E.,
755 Jaoui, M., and Hannigan, M. P.: Light absorption of organic carbon and its sources at a southeastern
756 U.S. location in summer, *Environ. Pollut.*, 244, 38-46, <https://doi.org/10.1016/j.envpol.2018.09.125>,
757 2019b.

758 Xie, M., Zhao, Z., Holder, A. L., Hays, M. D., Chen, X., Shen, G., Jetter, J. J., Champion, W. M., and
759 Wang, Q.: Chemical composition, structures, and light absorption of N-containing aromatic
760 compounds emitted from burning wood and charcoal in household cookstoves, *Atmos. Chem. Phys.*,
761 20, 14077-14090, 10.5194/acp-20-14077-2020, 2020.

762 Xie, M., Peng, X., Shang, Y., Yang, L., Zhang, Y., Wang, Y., and Liao, H.: Collocated measurements of
763 Light-absorbing organic carbon in PM_{2.5}: Observation uncertainty and organic tracer-based source
764 apportionment, *J. Geophys. Res. Atmos.*, 127, e2021JD035874,
765 <https://doi.org/10.1029/2021JD035874>, 2022.

766 Xu, Z., Feng, W., Wang, Y., Ye, H., Wang, Y., Liao, H., and Xie, M.: Replication Data for:
767 Underestimation of brown carbon absorption based on the methanol extraction method and its
768 impacts on source analysis, Harvard Dataverse, V2, <https://doi.org/10.7910/DVN/CGHPXB>, 2022.

769 Xu, L., Peng, Y., Ram, K., Zhang, Y., Bao, M., and Wei, J.: Investigation of the uncertainties of simulated
770 optical properties of brown carbon at two Asian sites using a modified bulk aerosol optical scheme
771 of the community atmospheric model version 5.3, *J. Geophys. Res. Atmos.*, 126, e2020JD033942,
772 <https://doi.org/10.1029/2020JD033942>, 2021.

773 Yan, F., Kang, S., Sillanpää, M., Hu, Z., Gao, S., Chen, P., Gautam, S., Reinikainen, S.-P., and Li, C.: A
774 new method for extraction of methanol-soluble brown carbon: Implications for investigation of its
775 light absorption ability, *Environ. Pollut.*, 262, 114300, <https://doi.org/10.1016/j.envpol.2020.114300>,
776 2020.

777 Yang, L., Shang, Y., Hannigan, M. P., Zhu, R., Wang, Q. g., Qin, C., and Xie, M.: Collocated speciation
778 of PM_{2.5} using tandem quartz filters in northern nanjing, China: Sampling artifacts and
779 measurement uncertainty, *Atmos. Environ.*, 246, 118066,
780 <https://doi.org/10.1016/j.atmosenv.2020.118066>, 2021.

781 Yu, Y., Ding, F., Mu, Y., Xie, M., and Wang, Q. g.: High time-resolved PM_{2.5} composition and sources
782 at an urban site in Yangtze River Delta, China after the implementation of the APPCAP,
783 *Chemosphere*, 261, 127746, <https://doi.org/10.1016/j.chemosphere.2020.127746>, 2020.

784 Zhang, A., Wang, Y., Zhang, Y., Weber, R. J., Song, Y., Ke, Z., and Zou, Y.: Modeling the global radiative
785 effect of brown carbon: a potentially larger heating source in the tropical free troposphere than black
786 carbon, *Atmos. Chem. Phys.*, 20, 1901-1920, 10.5194/acp-20-1901-2020, 2020.

787 Zhang, X., Hecobian, A., Zheng, M., Frank, N. H., and Weber, R. J.: Biomass burning impact on PM_{2.5}
788 over the southeastern US during 2007: integrating chemically speciated FRM filter measurements,
789 MODIS fire counts and PMF analysis, *Atmos. Chem. Phys.*, 10, 6839-6853, 10.5194/acp-10-6839-
790 2010, 2010.

791 Zhang, X., Lin, Y.-H., Surratt, J. D., and Weber, R. J.: Sources, composition and absorption Ångström
792 exponent of light-absorbing organic components in aerosol extracts from the Los Angeles basin,
793 *Environ. Sci. Technol.*, 47, 3685-3693, 10.1021/es305047b, 2013.

794 Zhu, C.-S., Cao, J.-J., Huang, R.-J., Shen, Z.-X., Wang, Q.-Y., and Zhang, N.-N.: Light absorption
795 properties of brown carbon over the southeastern Tibetan Plateau, *Sci. Total Environ.*, 625, 246-251,
796 <https://doi.org/10.1016/j.scitotenv.2017.12.183>, 2018.

Table 1. SEOC concentrations and extraction efficiencies (η , %) of total OC and OC fractions for different solvents.

OC prior to extractions	Water ^a	MeOH ^b	MeOH/DCM (1:1) ^b	MeOH/DCM (1:2) ^b	THF ^b	DMF ^a	
One-time extraction (N = 11)							
<i>SEOC, $\mu\text{g m}^{-3}$</i>							
Total OC	9.36 \pm 2.27	6.38 \pm 2.03	7.85 \pm 2.40	7.08 \pm 1.32	6.99 \pm 1.71	6.14 \pm 2.01	8.49 \pm 2.52
OC1	0.66 \pm 0.21	0.61 \pm 0.20	0.64 \pm 0.21	0.65 \pm 0.20	0.64 \pm 0.22	0.59 \pm 0.18	0.59 \pm 0.24
OC2	2.69 \pm 0.55	2.20 \pm 0.60	2.50 \pm 0.55	2.34 \pm 0.41	2.37 \pm 0.46	2.09 \pm 0.55	2.48 \pm 0.60
OC3	3.35 \pm 0.93	1.82 \pm 0.80	2.48 \pm 0.96	2.23 \pm 0.49	2.18 \pm 0.70	1.98 \pm 0.93	2.86 \pm 1.01
OC4	2.75 \pm 0.81	1.76 \pm 0.65	2.23 \pm 0.84	1.86 \pm 0.51	1.78 \pm 0.61	1.48 \pm 0.61	2.56 \pm 0.87
<i>η (%)</i>							
Total OC		66.7 \pm 8.58	82.3 \pm 8.68	76.0 \pm 7.70	74.3 \pm 7.83	64.2 \pm 8.08	89.0 \pm 7.96
OC1		91.7 \pm 4.85	96.1 \pm 6.73	97.9 \pm 5.02	97.4 \pm 4.35	89.6 \pm 9.55	88.8 \pm 4.98
OC2		80.8 \pm 8.11	92.7 \pm 3.69	87.7 \pm 5.87	88.5 \pm 7.21	76.9 \pm 7.62	91.4 \pm 6.17
OC3		52.4 \pm 11.8	73.0 \pm 11.5	68.1 \pm 8.64	65.2 \pm 10.2	57.6 \pm 12.0	84.3 \pm 9.79
OC4		63.3 \pm 9.13	80.3 \pm 11.4	69.0 \pm 9.26	64.5 \pm 8.11	52.7 \pm 5.86	92.8 \pm 9.69
Two-time extraction (N = 10)							
<i>SEOC, $\mu\text{g m}^{-3}$</i>							
Total OC	10.9 \pm 4.93	7.74 \pm 4.01	9.33 \pm 4.11	9.34 \pm 4.19	9.11 \pm 4.04	7.56 \pm 3.38	10.4 \pm 4.80
OC1	0.66 \pm 0.47	0.62 \pm 0.45	0.62 \pm 0.49	0.59 \pm 0.50	0.60 \pm 0.51	0.59 \pm 0.49	0.60 \pm 0.47
OC2	2.76 \pm 0.77	2.20 \pm 0.59	2.60 \pm 0.66	2.57 \pm 0.65	2.60 \pm 0.68	2.28 \pm 0.53	2.69 \pm 0.78
OC3	4.11 \pm 2.01	2.55 \pm 1.62	3.26 \pm 1.62	3.37 \pm 1.68	3.20 \pm 1.58	2.62 \pm 1.39	3.88 \pm 1.95
OC4	3.36 \pm 1.77	2.38 \pm 1.42	2.84 \pm 1.42	2.81 \pm 1.47	2.71 \pm 1.39	2.08 \pm 1.06	3.23 \pm 1.70
<i>η (%)</i>							
Total OC		69.9 \pm 5.88	86.6 \pm 7.86	86.2 \pm 8.73	84.8 \pm 7.76	70.1 \pm 8.01	95.6 \pm 3.67
OC1		93.6 \pm 4.08	90.3 \pm 13.9	82.6 \pm 25.9	83.8 \pm 22.4	82.9 \pm 15.1	92.2 \pm 13.9
OC2		80.1 \pm 5.01	94.8 \pm 4.20	93.6 \pm 4.94	94.7 \pm 2.51	83.5 \pm 6.86	97.2 \pm 2.12
OC3		59.0 \pm 10.6	80.0 \pm 10.2	82.3 \pm 9.86	79.1 \pm 10.6	63.9 \pm 10.7	94.2 \pm 4.15
OC4		69.3 \pm 6.46	86.3 \pm 12.0	84.3 \pm 12.0	82.7 \pm 13.3	62.9 \pm 7.76	96.9 \pm 5.18

^a Concentrations of rOC in extracted filters were measured after the baking process (100 °C, 2 h); ^b rOC was measured when extracted filters were air dried.

Table 2. Light-absorbing properties of SEOC following one-time and two-time extraction procedures.

Solvent	Water	MeOH	MeOH/DCM (1:1)	MeOH/DCM (1:2)	THF	DMF
One-time extraction						
Abs ₃₆₅ , Mm ⁻¹	5.13 ± 2.04	11.9 ± 5.83	10.3 ± 4.42	8.12 ± 3.38	5.48 ± 3.01	17.5 ± 8.05
Abs ₅₅₀ , Mm ⁻¹	0.35 ± 0.12	1.28 ± 0.87	0.97 ± 0.55	0.35 ± 0.47	0.42 ± 0.47	4.40 ± 2.34
MAE ₃₆₅ , m ² g ⁻¹ C	0.87 ± 0.19	1.46 ± 0.41	1.41 ± 0.36	1.13 ± 0.22	0.87 ± 0.25	2.02 ± 0.58
MAE ₅₅₀ , m ² g ⁻¹ C	0.062 ± 0.028	0.15 ± 0.084	0.13 ± 0.054	0.042 ± 0.52	0.059 ± 0.56	0.30 ± 0.12
Å	6.63 ± 0.49	5.44 ± 0.75	5.65 ± 0.54	6.59 ± 0.66	6.17 ± 0.69	4.52 ± 0.41
Two-time extraction						
Abs _{365,1st} , ^a Mm ⁻¹	6.64 ± 4.25	14.1 ± 7.09	14.6 ± 8.05	11.6 ± 6.78	7.17 ± 4.26	20.5 ± 10.6
Abs _{550,1st} , ^a Mm ⁻¹	0.42 ± 0.12	1.34 ± 0.70	1.34 ± 0.83	0.84 ± 0.50	0.53 ± 0.27	2.82 ± 1.44
Abs ₃₆₅ , ^b Mm ⁻¹	8.26 ± 5.21	15.5 ± 7.76	16.8 ± 8.82	14.0 ± 8.91	8.35 ± 4.81	21.9 ± 11.2
Abs ₅₅₀ , ^b Mm ⁻¹	0.50 ± 0.18	1.60 ± 0.78	1.64 ± 0.99	1.22 ± 0.98	0.69 ± 0.43	3.01 ± 1.49
MAE ₃₆₅ , m ² g ⁻¹ C	1.19 ± 0.26	1.70 ± 0.60	1.80 ± 0.52	1.50 ± 0.51	1.10 ± 0.40	2.11 ± 0.49
MAE ₅₅₀ , m ² g ⁻¹ C	0.082 ± 0.30	0.19 ± 0.11	0.17 ± 0.083	0.13 ± 0.069	0.094 ± 0.054	0.29 ± 0.075
Å	6.32 ± 0.58	5.37 ± 0.57	5.47 ± 0.67	5.57 ± 0.39	6.06 ± 0.54	4.53 ± 0.21

^a Light absorption coefficient of SEOC after the first extraction; ^b sum of SEOC absorption in 1st and 2nd extracts.

Table 3. Comparisons of light-absorbing properties of ambient PM_{2.5} extracts in DMF and MeOH derived from duplicate Q_f-Q_b data (*N* = 109).

	DMF			MeOH ^a		
	Median	Mean ± std	Range	Median	Mean ± std	Range
Abs ₃₆₅ , Mm ⁻¹	6.99	8.42 ± 5.40	1.14–30.8	5.59	6.43 ± 4.66	0.38–29.6
MAE ₃₆₅ , m ² g ⁻¹ C	1.13	1.20 ± 0.49	0.34–2.45	0.91	1.03 ± 0.58	0.089–2.49
Å	5.21	5.25 ± 0.64	3.21–6.82	6.49	6.81 ± 1.64	4.34–11.3

^a Data for MeOH extracts were obtained from Xie et al. (2022).

Figure 1

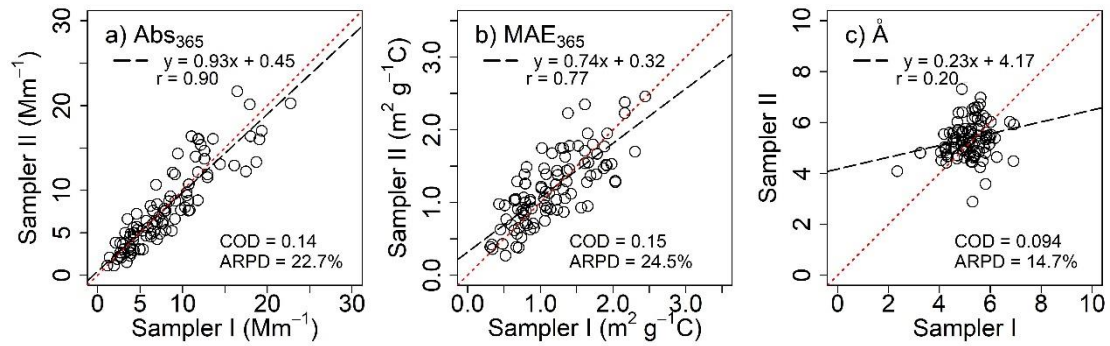


Figure 1. Comparisons between collocated measurements for light-absorbing properties of PM_{2.5} extracts in DMF after Q_b corrections.

Figure 2

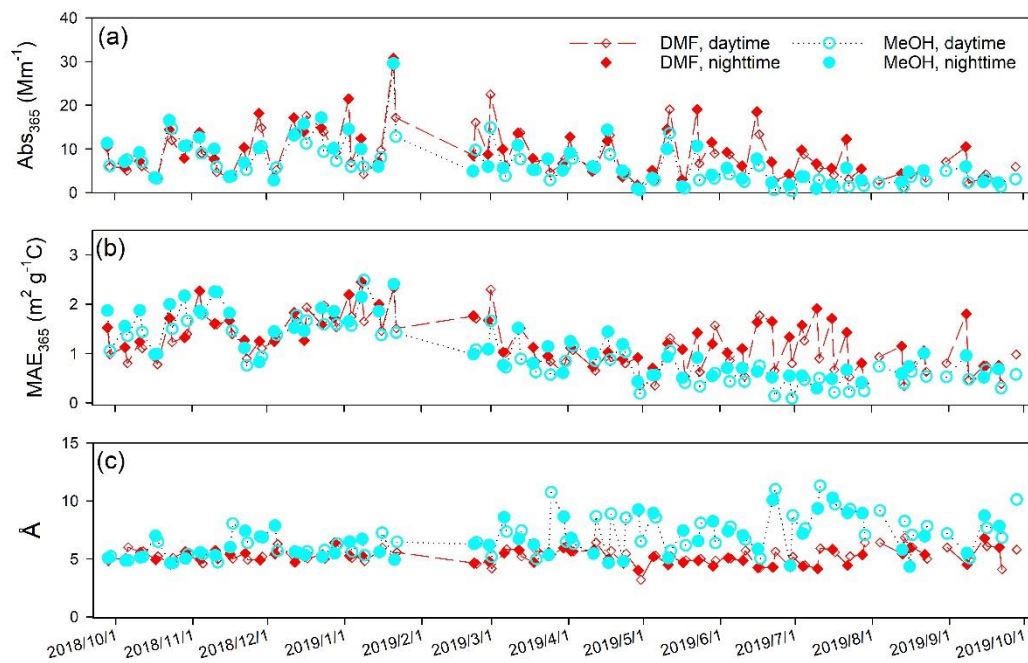


Figure 2. Time series comparisons of light-absorbing properties of DMF and MeOH extracts using artifact-corrected data. MeOH extract data were obtained from Xie et al. (2022).

Figure 3

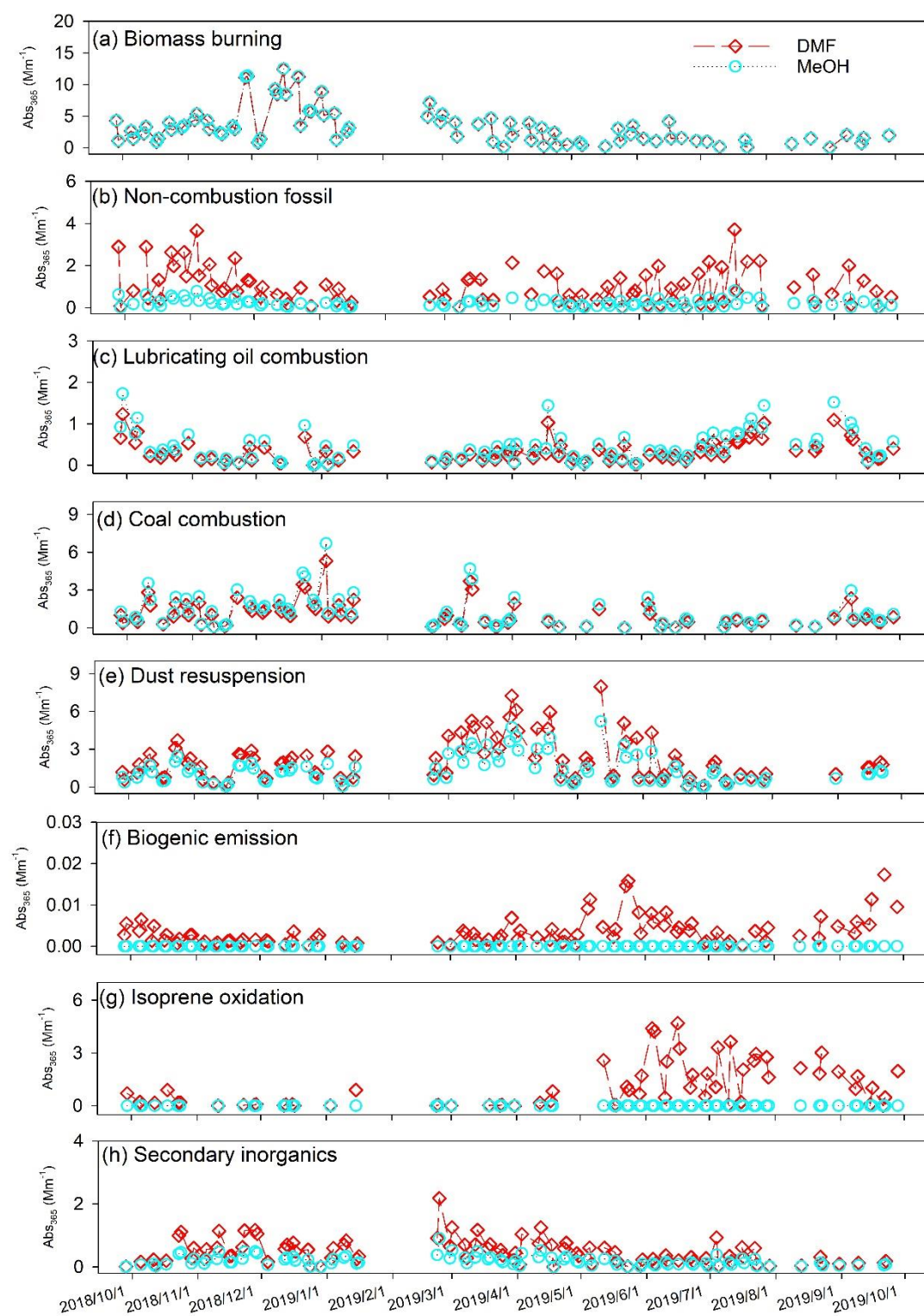


Figure 3. Time series of factor contributions to Abs_{365} of DMF and MeOH extracts of ambient PM_{2.5} samples.